0254-6124/2026/46(5)-1159-14 *Chin. J. Space Sci.* 空间科学学报

ZHANG Shun-Rong, COSTER Anthea J, AA Ercha, THAYYIL Jayachandran P, ZHANG Yongliang. Coupled Evolution of Storm-enhanced Density, Tongue of Ionization, and Polar Ionospheric Hole during the 10 May 2024 Superstorm. *Chinese Journal of Space Science*, 2026, **46**(5): 1159–1172. CSTR:32142.14.cjss.2026–0019. DOI:10.11728/cjss2026.05.2026–0019

Coupled Evolution of Storm-enhanced Density, Tongue of Ionization, and Polar Ionospheric Hole during the 10 May 2024 Superstorm

ZHANG Shun-Rong[1] COSTER Anthea J[1] AA Ercha[1]

THAYYIL Jayachandran P[2] ZHANG Yongliang[3]

1(*Haystack Observatory*, *Massachusetts Institute of Technology*, *Westford*, *MA* 01886)

2(*Physics Department*, *University of New Brunswick*, *Fredericton*, *NB E3B 5A3*)

3(*Applied Physics Lab*, *Johns Hopkins University*, *Laurel*, *MD* 20723)

Abstract This study investigates the concurrent evolution of subauroral Storm-Enhanced Density (SED), the polar Tongue of Ionization (TOI), and the Polar Ionospheric Hole (PIH) during the 10 May 2024 geomagnetic superstorm. Using global GNSS Total Electron Content (TEC) and TIMED/GUVI thermospheric $[O]/[N_2]$ ratio measurements, we focus on the interplay between ionized and neutral density structures at polar latitudes. Our observation exhibited the following scenario that highlights the new understanding of peculiar $[O]/[N_2]$ influences on TOI and plasma patches during this storm. (i) With the arrival of the ICME shock and subsequent Interplanetary Magnetic Field (IMF) B_z southward turning, Prompt Penetration Electric Field (PPEF) drove Equatorial Ionization Anomaly (EIA) crests moving poleward, causing a mid-latitude density enhancement. At midlatitude, the poleward Subauroral Polarization Stream (SAPS) provided significantly intensified sunward flow, while PPEF generated poleward flow, thus the two ion drift components led to the buildup of high electron density, forming the SED base and plume. (ii) At noon, the SED plume was entrained into the anti-sunward flow channel toward the polar cap. (iii) An unusual dayside PIH was formed as the neutral gas with a depleted $[O]/[N_2]$ ratio began circulating in the morning sector toward afternoon. This presumed neutral circulation was primarily driven by the increased ion drag associated with significant storm-time auroral electric fields. (iv) Fresh TOI plasma is moving into the polar cap and rotating eastward, with some portion continuing antisunward convecting. Successively following the TOI eastward convection, the PIH also rotates eastward. (v) PIH and TOI continued to be depleted, with TOI being segmented, as the entire polar cap was soaked by the substantially suppressed $[O]/[N_2]$ air. The TOI and PIH remained eastward convicting for several hours, including a 2 h interval of larger positive IMF B_y.

Key words Tongue of ionization, Storm-enhanced density, Plasma patches, Thermospheric composition ($[O]/[N_2]$), Magnetosphere-ionosphere-thermosphere coupling, Geomagnetic storms

Classified index

1 Introduction

In the high-latitude ionosphere, large-scale plasma structures serve as critical indicators of coupled Magnetosphere-Ionosphere-Thermosphere (M-I-T) dynamics. Among them, the Tongue of Ionization (TOI) is a promi-

Received

©The Author(s) 2026. This is an open access article under the CC-BY 4.0 License (https://creativecommons.org/licenses/by/4.0/)

nent feature characterized by a narrow channel of enhanced F-region plasma density extending from the dayside subauroral ionosphere into the polar cap. TOIs are typically formed during geomagnetic storms when sunward-convecting plasma from Storm-Enhanced Density (SED) plumes is fed into high-latitude convection pathways under sustained southward Interplanetary Magnetic Field (IMF) conditions[1−4]. SED plumes themselves are robust midlatitude electron density enhancements driven by storm electric fields and transport processes, with their evolution and connection to polar cap features, such as TOI and patches, extensively documented[5−8]. These features can span thousands of kilometers and persist for hours, contributing significantly to ionospheric mass transport across the polar cap and into the nightside high-latitude region.

The morphology and occurrence of both SED and TOI are highly variable and influenced by the background state of the ionosphere, solar wind driving conditions, and likely thermospheric composition variability. Specifically, SED is tightly connected with storm-time electric fields inside the polar region and their penetration into lower latitudes, Subauroral Polarization Streams (SAPS)[9−11], and other related magnetosphere-ionosphere-thermosphere coupling processes[8]. It is believed that TOI formation and evolution depend on both horizontal plasma transport and vertical lifting due to electric fields and wind surges[4,6]. SED and TOI observational signatures have been identified across GNSS Total Electron Content (TEC), incoherent scatter radar, and satellite *in-situ* data[5,7,12−16]; first-principal model-based simulations have reproduced the TOI's elongation, density structure, and its coupling with the polar cap convection pattern[4,17−20].

When the elongated stream of plasma, the TOI, is convected antisunward into the polar cap via $\boldsymbol{E} \times \boldsymbol{B}$ drift driven by high-latitude electric fields[21,22], it is often segmented into discrete polar cap patches, which are localized islands of enhanced electron density[1,2,21,23]. These patches typically form due to temporal and spatial fluctuations in the IMF, particularly under southward B_z conditions with varying B_y, which distort convection patterns and fragment the TOI[24−26]. Both TOIs and polar cap patches are key contributors to polar ionospheric variability, producing sharp density gradients that can drive plasma instabilities and irregularities and GNSS scintillations[13,27,28].

A related but distinct phenomenon is the neutral tongue, a region of altered thermospheric composition, most notably enhanced $[O]/[N_2]$ ratio, that is convected into the polar cap in parallel with ionized structures like the TOI. According to Ref. [29], it forms when parcels of neutral air rich in molecular species (high $[O]/[N_2]$) are transported antisunward across the polar cap by the thermospheric neutral wind pattern, which follows the high-latitude convection flow. This neutral transport mechanism is structurally similar to the ion transport that convects the TOI. Compared with TOI, the neutral tongue tends to be weaker, extends a shorter distance across the polar cap, and requires more time to develop. Observational evidence provided by Ref. [30] supports the existence of neutral composition structures near subauroral latitudes.

The development of high $[O]/[N_2]$ is totally different from the $[O]/[N_2]$ depletion that constitutes the composition disturbance zone, which occurs initially at auroral latitudes but then expands to mid-and low latitudes, causing the negative phase of storms[31].

In contrast, Polar Ionospheric Holes (PIHs), the electron density depletion, are regions of un-usually low electron density, frequently observed in the polar cap during geomagnetically quiet periods or polar night. These holes arise from a combination of weak ionization sources (due to the absence of solar EUV radiation) and elevated recombination rates; meanwhile, slow plasma convection allows sustained ion loss by chemistry, particularly under conditions of low $[O]/[N_2]$ ratios[32,33]. While often less dynamic than TOIs, polar holes exhibit sharp horizontal density gradients and can persist for long durations in the central polar cap. These features are not passive but interact with surrounding plasma structures, including TOIs. When TOIs encounter density depletion holes, the resulting steep electron density gradients may drive plasma irregularities or fragmentation into polar cap patches, with implications for GNSS (Global Navigation Satellite System) signal integrity and space weather effects[27,34,35].

SED, TOI, Patches, and PIH are distinctive ionospheric density gradient structures that exhibit substantial variability across diverse storm conditions. On

10 May 2024, it presents another rare opportunity to investigate the dynamical behaviors of these plasma density structures in the polar cap region. As demonstrated in this study, the simultaneous plasma and neutral disturbances significantly shape the stormtime upper atmosphere in the polar region, a coupling aspect that hasn't been frequently observed in prior research. The only relevant polar cap research conducted for this event was by Ref. [36], who provided a comprehensive synoptic, multi-instrument characterization of the polar ionosphere's response throughout the storm's expansion, main, and recovery phases using a suite of observations, including GNSS TEC, Incoherent Scatter Radar, and ionosonde measurements at high latitudes. Our study focuses on how the TOI and PIH evolve during the concurrent neutral gas development with depletion of the composition ratio [O]/[N_2].

2 Observation and Data

2.1 GNSS TEC Data Processing

The Massachusetts Institute of Technology (MIT) Haystack Observatory has continuously produced worldwide ground-based GNSS vertical TEC data since 2000 using the MAPGPS (MIT Automated Processing of GPS) software suite[37,38]. These data are freely accessible to the community through the Madrigal database*. GNSS TEC processing currently utilizes more than 6000 global receivers, generating approximately 150 million Line-Of-Sight (LOS) data points daily[39]. These data are contributed by international research communities. For example, the Canadian High Arctic Ionospheric Network (CHAIN) is a distributed array of ground-based radio instruments located in the Canadian High Arctic, including high data-rate GNSS scintillation and TEC monitors in the cusp, auroral oval, and polar cap regions[40]. These and other high-latitude GNSS observations were used in this study.

In addition to TEC values, this study also demonstrates the fluctuation component of TEC derived after detrending the background vertical TEC, following the widely adopted approach first proposed by Ref. [41] and later applied in numerous TID studies[42–45]. Here we utilized a low-pass Savitzky-Golay filter[46] with a linear basis function and a 30-minute sliding window to determine the smooth background[8,45,47–50]. This filter applies a convolution process with least-squares fitting over time-adjacent data subsets for each satellite-receiver pair.

2.2 Thermospheric Composition and TIMED/GUVI

During geomagnetic storms, the thermospheric composition undergoes significant redistribution, leading to changes in the column-integrated [O]/[N_2] ratio. These changes are primarily driven by high-latitude heating and upwelling, which bring molecular-rich (N_2-dominant) air into the F region. As a result, the [O]/[N_2] ratio typically decreases in regions affected by this composition disturbance. A lower [O]/[N_2] ratio enhances ion loss through recombination, contributing to negative ionospheric storms in which electron density is reduced despite continued solar EUV input.

The Global Ultraviolet Imager (GUVI) onboard the TIMED satellite has been essential for detecting these changes by providing global-scale observations of storm-time thermospheric composition variations. The TIMED (Thermosphere-Ionosphere-Mesosphere Energetics and Dynamics) satellite, launched by NASA in 2001, is designed to study the dynamics, composition, and energy inputs of the mesosphere and lower thermosphere. It operates in a low Earth orbit at an altitude of approximately 625 km with a 97.1° inclination, enabling near-global coverage over time. TIMED's orbital configuration allows sampling of all local times (~08:30 during the May storm) over a 60-day period due to its processing, sun-synchronous-like orbit. One of its key instruments is GUVI, which measures Far-Ultraviolet (FUV) emissions to infer thermospheric composition and structure[51]. GUVI observes in the 115–180 nm wavelength range, capturing emissions from both atomic oxygen and molecular nitrogen. A primary GUVI data product is the column-integrated [O]/[N_2] ratio, which serves as a proxy for thermospheric composition. This ratio is derived from measurements of atomic oxygen emissions at 130.4 nm and 135.6 nm and N_2 Lyman-Birge-Hopfield (LBH) band emissions, processed through photochemical modeling and inversion algorithms[52,53]. In the auroral region O and N_2 FUV emis-

* http://openmadrigal.org

sion retrievals may be affected by intense auroral emissions; however, this study focuses on significant depletion features of the ratio [O]/[N_2] that are generally more robust and less likely to be dominated by such effects.

3 Results and Analysis

3.1 Solar Geophysical Conditions and Global TEC Responses

The 10 May 2024 superstorm was the most intense geomagnetic storm of the past two decades. The solar-geophysical conditions, as shown in Figure 1, were characterized by a substantial decrease in the *Dst* (Sym-*H*) index, which plummeted to nearly −500 nT at approximately 02:00 UT on 11 May. This decrease was preceded by an abrupt positive excursion around 17:00 UT on 10 May, indicating the arrival of the shock front associated with the Interplanetary Coronal Mass Ejection (ICME) at the magnetopause. Following the shock arrival, the solar wind dynamic pressure surged to approximately 50 nPa, and the IMF B_z component turned strongly southward, leading to significant magnetospheric compression. The southward B_z excursion reached values between −35 and −39 nT at approximately 18:00 UT and again near 22:00 UT, followed by a subsequent rotation to strongly northward conditions of up to +50 nT. Notably, during this interval, B_z experienced a dramatic northward enhancement exceeding +75 nT that persisted for nearly three hours.

The ionospheric TEC response was prompt, global, multiscale, dynamic, and complex. Figure 2 illustrates TEC variations (Figure 2a, d) along the great meridians of approximately 70°W in the Western Hemisphere (eastern American sector) and 110°E in the Eastern Hemisphere (eastern Asian sector). TEC relative variations (Figure 2b, e) represent percentage changes relative to a quiet day, 9 May 2024. dTEC represents ionospheric fluctuations (Figure 2c, f). It was evident that the prompt response spanned both day and night, with TEC, and more prominently dTEC, being enhanced during daytime and depleted at night. The response was particularly intense at midlatitudes during the day and at equatorial latitudes at night. These features were clear signatures of TEC changes driven by prompt penetration of the Interplanetary Electric Field (IEF) as demonstrated in Ref. [54].

The IEF sudden imposition on the magnetospheric and ionospheric current systems caused deep penetration of the electric field into low latitudes, leading to upward perpendicular-to-B (PerpB) plasma drift on dayside and downward PerpB drift on nightside. TEC increased on dayside as a result of this upward drift, combined with continuous replenishment of bottomside ionization by photochemical production. In contrast, TEC decreased at night due to sustained downward drift, which facilitated efficient chemical recombination loss.

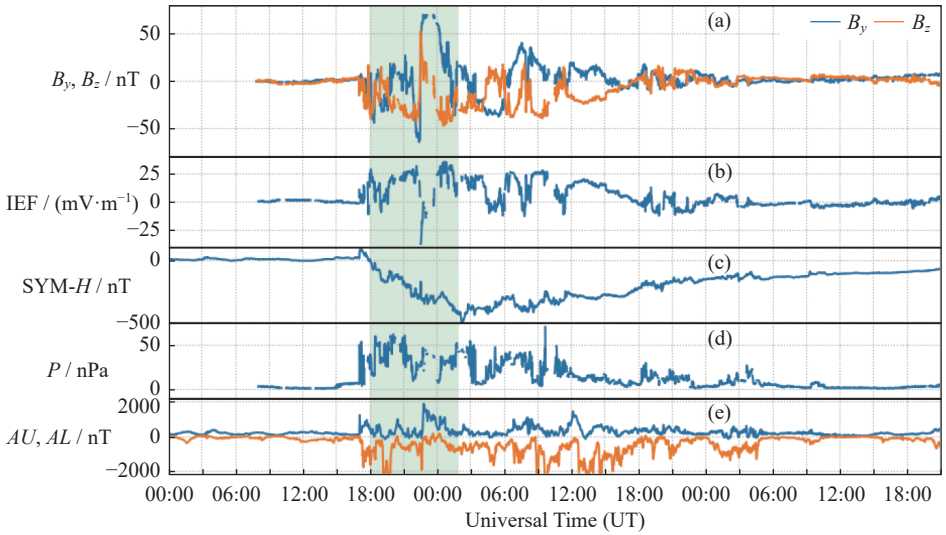


Fig. 1 Solar geophysical conditions for 10–12 May 2024. IMF B_y and B_z (a), interplanetary electric field (b), SYM-*H* index (c), solar wind dynamic pressure (d), auroral *AU* and *AL* index (e)

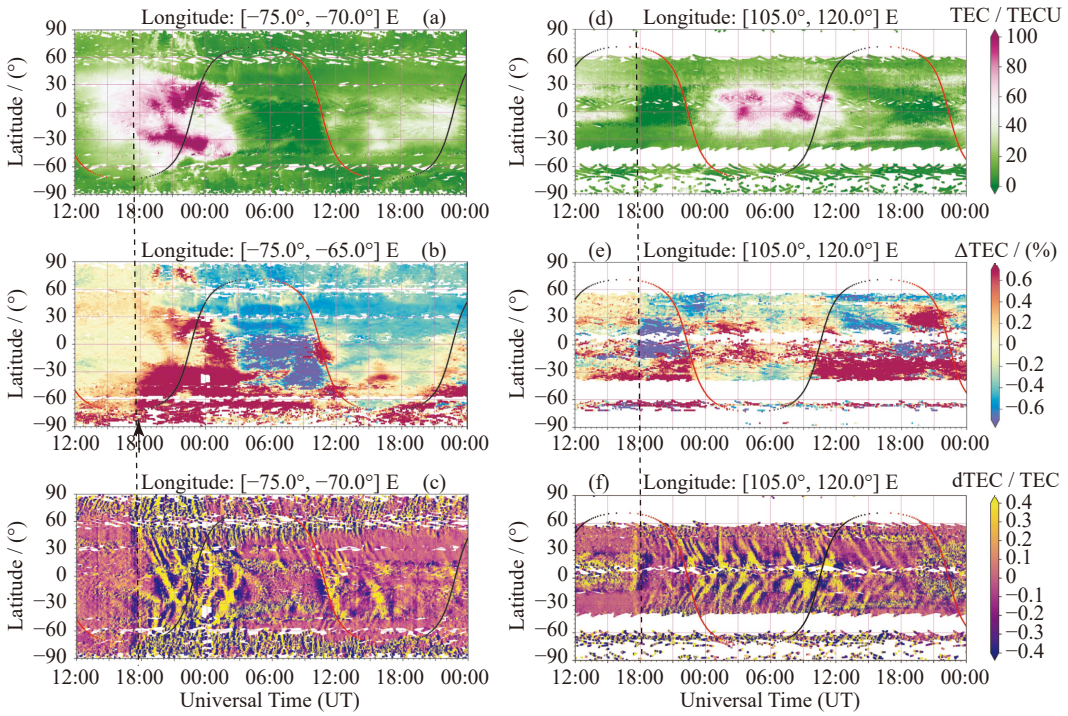


Fig. 2 Latitudinal and UT variations in TEC (TECU, a and d), TEC relative changes (percentage fraction) from the reference on 10 May 2024 (b and e), and dTEC (TECU, c and f) in American (left panels) and Asian (right panels) sectors which have 12-hour local time offset. Dashed lines mark the ICME arrival induced simultaneous ionospheric variations

This prompt-penetration electric field (PPEF) effect on TEC during shock arrival has been a commonly observed ionospheric phenomenon. The PPEF was measured directly by the incoherent scatter radar at Sanya[55].

Immediately following the shock arrival, Traveling Ionospheric Disturbances (TIDs) were generated (Figure 2c, f), accompanied by TEC depletion that initiated at high latitudes and propagated toward lower latitudes. The TIDs appeared to emanate from a source region located near ~60°N in the eastern American sector. Equatorward propagation was particularly prominent during daytime in the eastern American sector, with phase speeds of approximately 600 m·s^{-1}. In the eastern Asian sector (nightside), simultaneous TID propagation was also observed, exhibiting smaller absolute amplitudes but comparable relative amplitudes when compared with those in the eastern American sector. TIDs also propagated across equatorial latitudes into the opposite hemisphere.

TEC depletion exceeded 100% in the southern hemisphere on the nightside in the eastern American sector (Figure 2b), where the negative phase persisted for several days. In contrast, the negative phase was less pronounced in the eastern Asian sector relative to the quiet-day reference, but intensified during nighttime on 11 May (Figure 2e), consistent with the findings of Ref. [56]. In addition, a notable TEC enhancement island was observed over eastern Asian midlatitudes between 18:00 and 21:00 UT[57,58], exhibiting slow zonal propagation.

3.2 Storm Enhanced Density

SED began to occur at ~18:00 UT soon after the ICME arrival and moved out of GNSS data coverage over the contiguous United States (CONUS) by the end of the UT day on 10 May. Figure 3 illustrates the development of the SED in terms of both absolute and relative TEC differences with respect to the reference day, May 9. These quantities are denoted as ΔTEC and ΔTEC %, respectively. The SED initially appeared as a highly localized enhancement in the midlatitude region (~60° apex latitude) near the noon sector (Figure 3a'). During the subsequent four hours, the enhancement zone expanded both zonally and meridionally, while the main body of the structure migrated westward/sunward and poleward (see also Figure 4). The westward migration speed was approximately 95 m·s^{-1}, which was slower than the

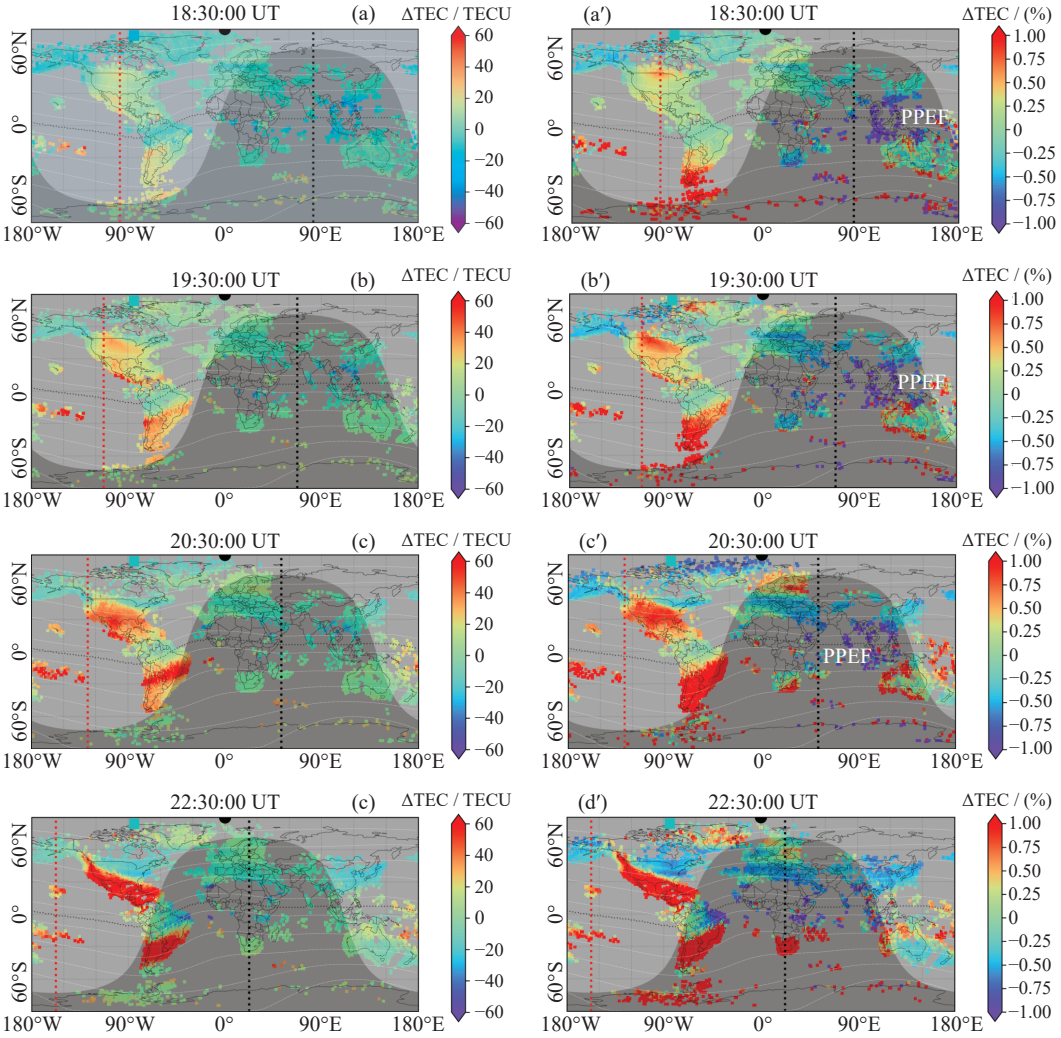


Fig. 3 A sequence of global TEC maps to demonstrate the SED development. TEC variations are shown as absolute difference from the reference day 10 May 2024 (left) and relative percentage (fractional) change (right)

Earth's rotation speed, indicating sub-rotational motion. The SED enhancement structure was tilted in a northwest–southeast orientation, with the plume extending toward the noon sector at higher latitudes into the auroral and cusp regions. The SED plume became pronounced by 20:30 UT and was significantly enhanced by 22:30 UT, reaching amplitudes of approximately 60 TECU, or ~80% above the background level. Along this tilted structure, density depletion developed toward the duskside and gradually intensified, suggesting the formation and motion of the midlatitude trough.

The impact of PPEFs on SED initiation was evidently accompanied by sudden changes in the equatorial region. By 19:30 UT, the southern crest of the Equatorial Ionization Anomaly (EIA) in South America had already moved beyond the 15° S apex latitude, registering TEC enhancements of approximately 30 TECU, or ~80% above the background level (Figures 3b and 3b'). In contrast, equatorial TEC depletion was present but of smaller magnitude. On nightside, however, TEC reduction was much more pronounced, particularly in relative changes (Figures 3a' and 3b'). These equatorial TEC variations were driven by PPEFs, which were eastward on dayside and westward on nightside, thereby producing upward and downward vertical ion drifts, respectively.

The dayside PPEF over the American sector drove upward ion drift at the magnetic equator, and poleward (PerpB) and upward plasma drifts at midlatitudes. As a combined consequence of the enhanced fountain effect

and local PPEF forcing, plasma was transported poleward into midlatitudes and upward to higher altitudes. This uplifted plasma formed the lower latitude base of the SED plume. The westward-tilted TEC enhancement structure was likely related to westward plasma flow that varied with latitude. This flow was driven either by Subauroral Polarization Streams (SAPS) or by the penetration and expansion of the two-cell convection electric field, which is poleward in the afternoon-dusk sector and drives westward ion drift. Consistent with this interpretation, SAPS was indeed observed by the DMSP drift meter[16].

3.3 Polar Tongue of Ionization and Ionization Hole

As illustrated in Figure 4, the SED plume plasma, together with auroral plasma in the cusp, was eventually entrained into the antisunward convection channel within the polar cap. A sequence of polar-view TEC maps, spanning from 17:00 UT on 10 May prior to the ICME arrival (Figure 5) to 08:55 UT on the following day (Figure 6), during the deep recovery phase of the storm, was used to demonstrate the evolution of Tongue of Ionization (TOI) structures and their interaction with the Polar Ionospheric Hole (PIH), as well as the influence of neutral composition changes.

SED signatures in the polar-view maps first became evident at 18:00 UT, and the plume reached apex latitudes exceeding 65°N by 18:45 UT. Prior to this, however, localized density depletion was identified at approximately 18:15 UT near 08:00 LT within the >65° N apex latitude region. More widespread depletion had begun even earlier, around 18:00 UT, coincident with [O]/[N_2] depletion measured by TIMED/GUVI. Concurrent TOI and PIH structures were observed at 19:00 UT. By 19:30 UT, TEC depletion associated with the PIH appeared to segment the TOI; at this time, the PIH was well correlated with measured [O]/[N_2] depletion. Notably, the PIH rotated anticlockwise (eastward) across the noon sector into the afternoon sector throughout the interval from 18:15 to 21:30 UT shown in Figure 5. Owing to the influence of the low-density PIH, the TOI occupied only a limited region of the polar cap and behaved more like discrete patches. An isolated patch was observed between 20:00 and 21:00 UT in the afternoon sector. At 21:15 UT and 21:30 UT, TOI plasma continued to enter the polar cap on the dayside, where PIH-related depletion was less severe than on the nightside, consistent with the measured [O]/[N_2] depletion. The TOI reached the magnetic pole by 21:30 UT.

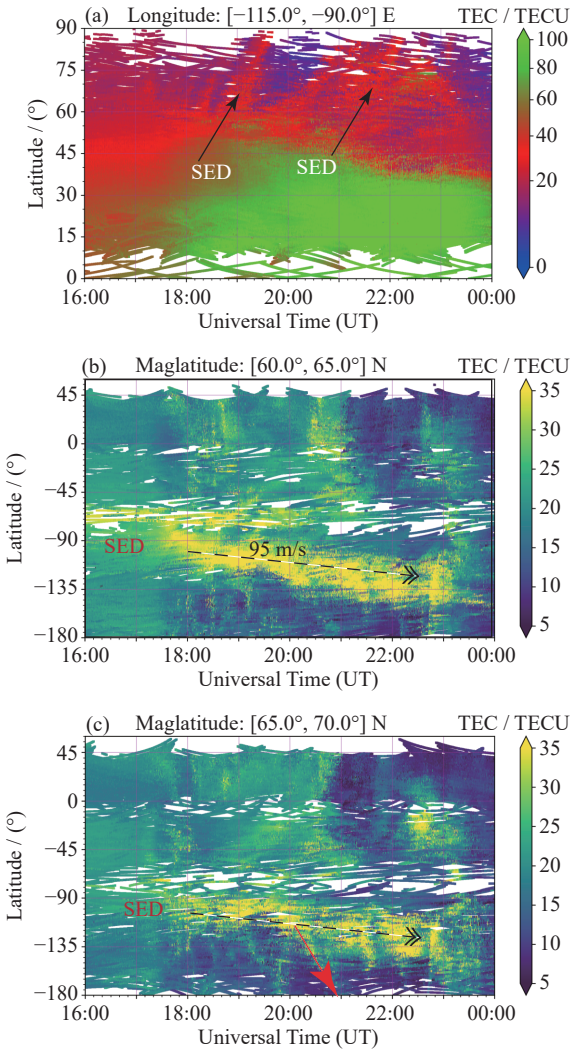


Fig. 4 SED plume temporal evolution in latitude for a broad longitude bin −115°E to −90°E degrees (a), and in longitude at 60°N–65°N Apex latitude (b), and at 65°N–70°N Apex latitude (c) on 10 May 2024

During the subsequent interval from 21:45 UT to 23:00 UT (Figure 6), the TOI remained intense. This period coincided with the northward turning of IMF B_z and a strongly positive IMF B_y. The eastward convection of both TOI and PIH in the dusk sector remains steady. After this interval, no additional TOI structures or patches were discernible within the polar cap, even though SED activity persisted until approximately 02:00 UT. From 00:00 UT onward, the entire polar cap was dominated by TEC suppression associated with [O]/[N_2] depletion for

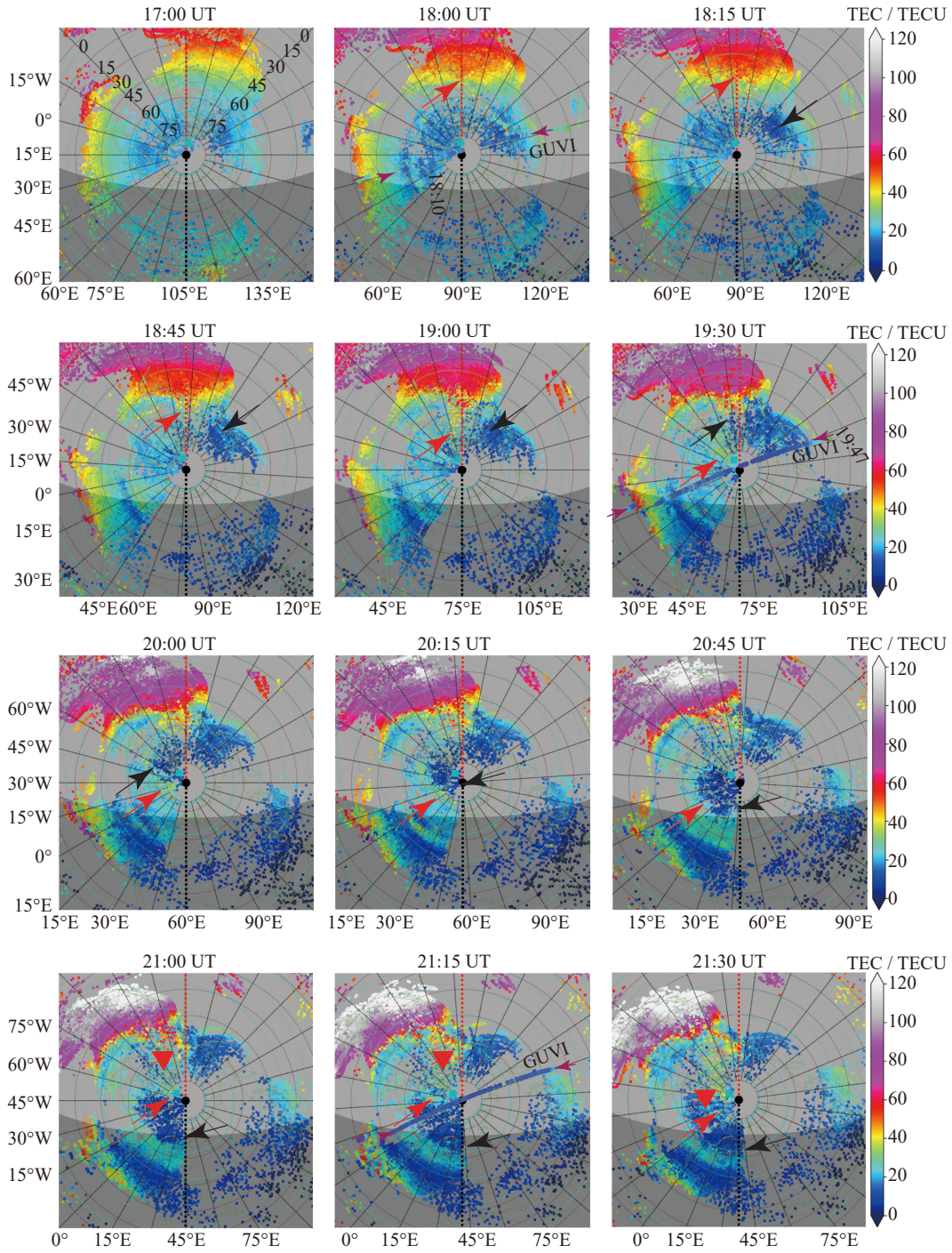


Fig. 5 A polar view of TEC snapshots between 17:00–21:30 UT on 10 May 2024 to demonstrate the plasma density gradients TOI or the patch (see red arrows) and Polar Ionization Hole (back arrows). Corresponding GUVI [O]/[N_2] variations along the trajectory of the TIMED are also shown at approximate times of TEC snapshots. Note that the depletion of [O]/[N_2] inside the polar cap does not align with the region of enhanced TEC, which would suggest auroral precipitation

several hours, as shown in Figure 6. Nevertheless, TEC enhancements were observed over auroral latitudes (~60°N apex latitude) at 02:06 UT, 07:00 UT, and 08:55 UT on the nightside (see yellow arrows); these auroral precipitation features[59] were not associated with TOI nor polar cap patches.

To summarize the TOI and PIH variations, Figure 7 traces their temporal evolution at two apex latitude

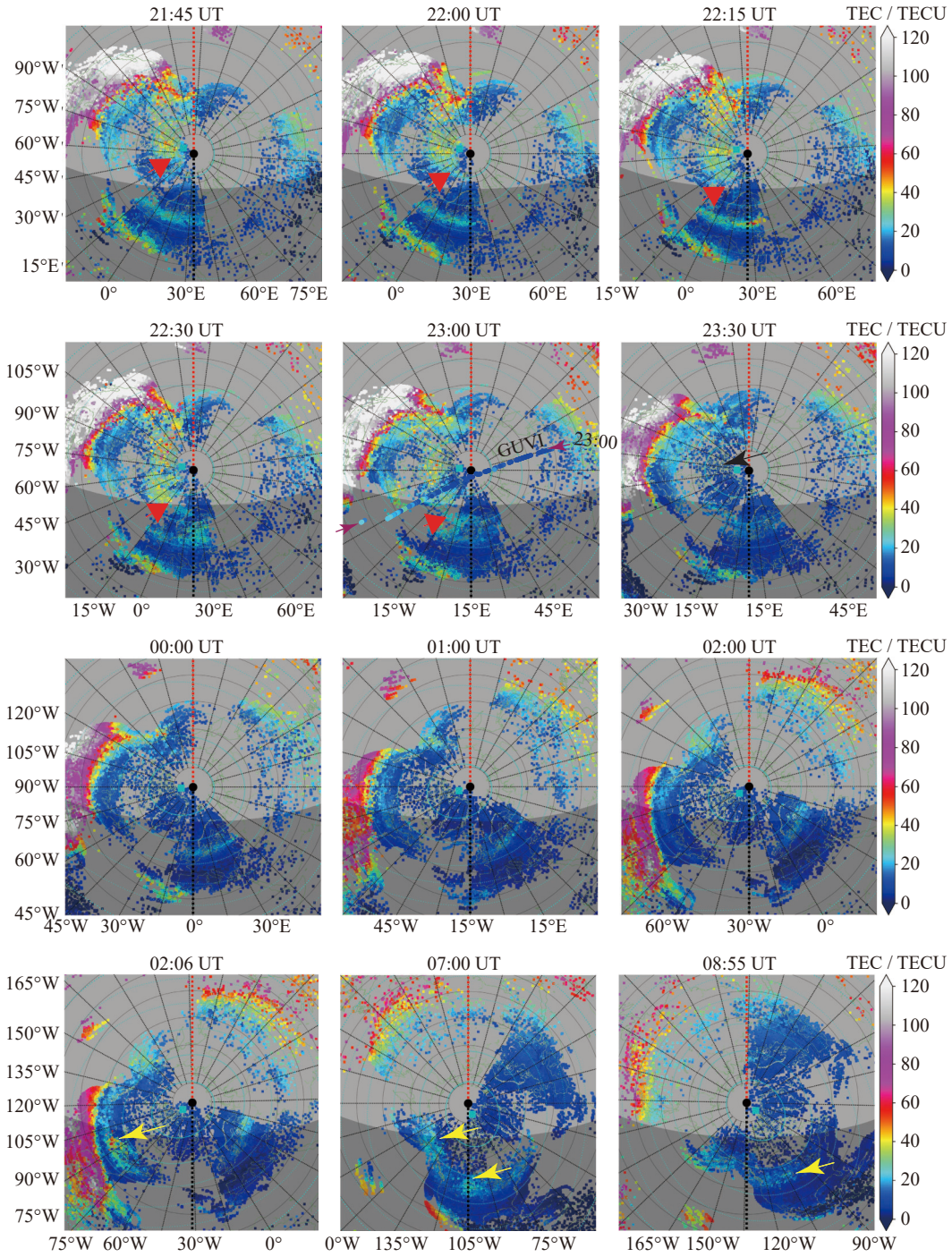


Fig. 6 Same as Figure 5 but for snapshots at 21:45–08:55 UT (10–11 May 2024). Yellow arrows mark the area of enhanced TEC due to auroral particle precipitation

bands, 70°N–75° N and 75°N–80° N. The TOI propagated eastward in the dusk sector at a speed of approximately 700 m·s^{-1} and westward in the dawn sector (Figures 7a, b). These propagation directions were largely consistent with the antisunward plasma flow in the polar cap. While the TOI generally convected eastward and antisunward into the polar cap, the PIH appeared to have followed the TOI dynamics, with a much deeper depletion at higher apex latitudes (75°N–80°N) than at 70° N–75°N where some plasma cloud remained (Figures 7a,b).

The PIH convected eastward on the duskside at ap-

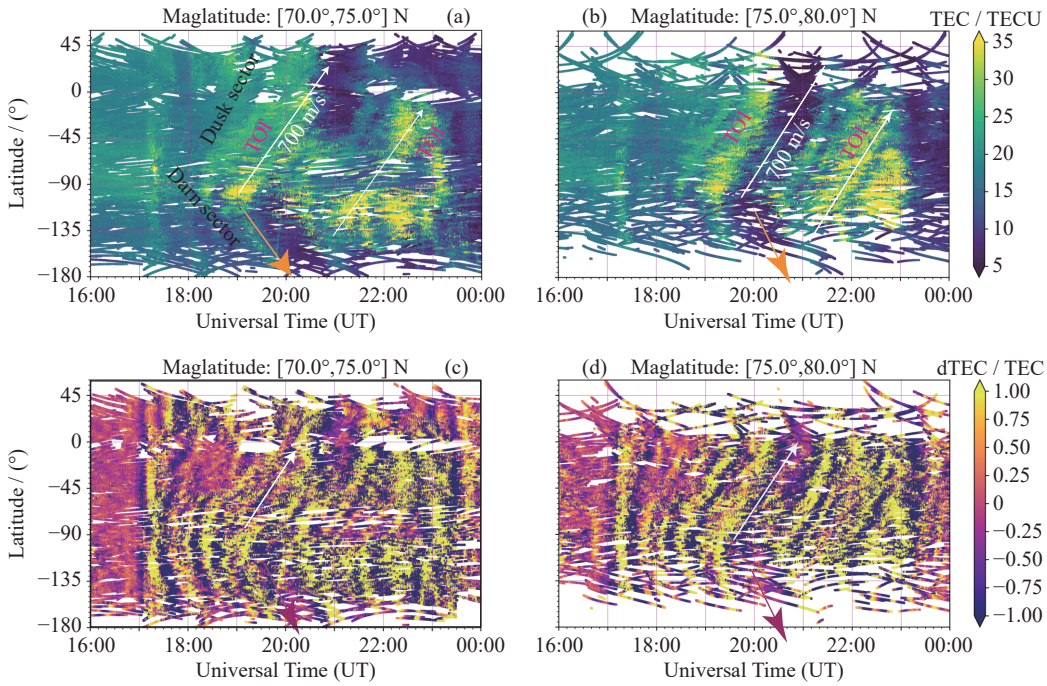


Fig. 7 Longitudinal propagation inside the polar cap of density structures in TOI and patches (a and b), and dTEC fluctuations (c and d) over two apex latitude bins of 70°N–75°N (left) and 75°N–80°N (right) on 10 May 2024

proximately the same speed as the TOI. This may imply that the high latitude $\boldsymbol{E}\times\boldsymbol{B}$-driven convection was so strong that neutrals were also convicting at the similar speed such that the [O]/[N_2] depletion gas has sustained chemical impact on O^+ reduction, causing PIH which was convecting along with TOI. The differential TEC (dTEC), representing the fluctuation component of TEC, propagated together with the bulk TOI flow (Figures 7c, d). The slopes of the dTEC fronts consistently corresponded to a convection speed of ~700 m·s^{-1} within the polar cap. In addition, dTEC exhibited clear small structures superposed on the PIH region, particularly at higher latitudes (Figure 7d).

In the preceding discussion, it was observed that PIH is associated with the depletion of [O]/[N_2]. The variations in [O]/[N_2] for each orbit are presented in Figure 8 over the two days. The [O]/[N_2] depletion became severe at the 21:24 UT orbit (Figure 8a) and subsequent orbits (Figure 8b). This depletion of neutral gas can lead to a reduction in O^+ due to enhanced recombination with N_2 and a decrease in O^+ photoionization on the sunlit ionosphere as O decreases. The impact is particularly pronounced on the dayside due to the combination of reduced O and the increase in N_2. The O^+ plasma entering this throat region as TOI is subject to this chemical effect, resulting in segmentation of TOI and the development of patches. While the neutral gas with depleted [O]/[N_2] convects at a similar speed to the O^+ ions, the sustained chemical influence can be effective in reducing O^+. This [O]/[N_2] influence extends beyond PIH and affects TOI as well. The exact consequences on plasma density depend on the convection and circulation of plasma and neutrals, as well as their time history, particularly when the IMF B_z and B_y are subject to dynamic development. In conclusion, additional consideration of the influences of [O]/[N_2] depletion can contribute to the TOI segmentation and patch formation.

3.4 Highlights of Observational Features

The observations presented here underscore the extreme nature of the May 2024 superstorm and its profound impact on the M-I-T system. The prompt global TEC response, characterized by dayside enhancements and nightside depletions, confirms the dominance of PPEF mechanisms during the initial phases of such intense events. The subsequent development of TIDs propagating from high to mid-latitudes demonstrates the efficient transfer of energy from the auroral regions into the global ionosphere. Main observational features are summa-

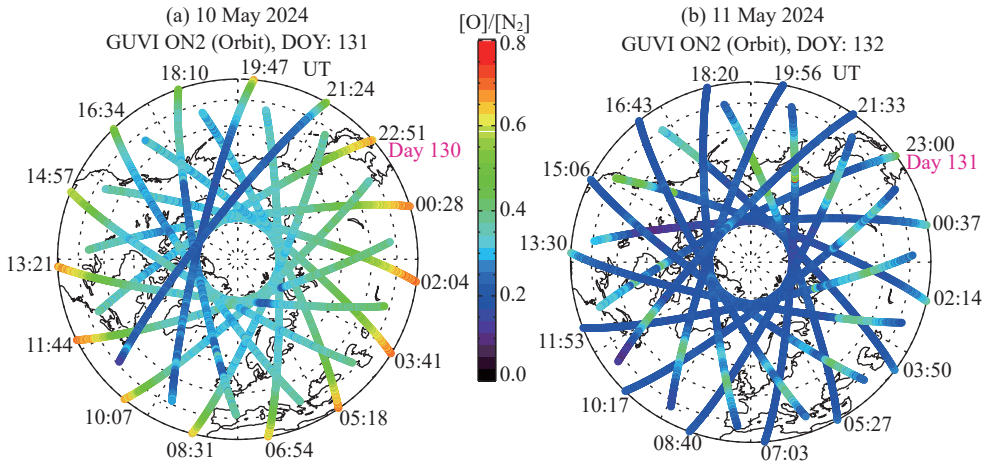


Fig. 8 A polar view of the GUVI [O]/[N_2] measurements at ~08:30 LT on 10−11 May 2024. Orbit-by-orbit variations is shown in the left panels; a smoothed version to fill the gaps is provided merely to show a big and rough picture of [O]/[N_2] distribution in the polar region

rized as follows.

(1) A well-defined SED plume formed in the mid-latitude noon sector, expanded northwestward, and propagated sunward and poleward at a subrotational speed.

(2) The SED plume fed into the polar convection pathway, contributing the formation of TOI that initially convected antisunward through the throat region and then eastward into afternoon and dusk sectors inside the polar cap.

(3) Almost simultaneously, a PIH emerged at polar latitudes and rotated and propagated eastward along with the TOI which was effectively segmented into patch-like structures.

(4) The PIH was observed accompanying the neutral air with depletion of the [O]/[N_2] ratio, implying the significance of composition-driven contribution to electron density reduction. The presumed neutral circulation under the influence of ion convection has a sustained chemical impact on the convecting ionospheric density, including TOI. This PIH observation appears substantially different from what has often been observed on the nightside without solar photoionization during magnetic quiet time with slow plasma convection[60].

(5) dTEC observations captured fine-scale irregularities within the TOI and PIH, demonstrating multi-scale plasma density structures.

(6) The suppression of TOI after 23:00 UT, despite ongoing SED activity, emphasizes the impact of sustained [O]/[N_2] depletion on plasma structure sustainability.

Based on these observations, we will outline a general scenario in the subsequent Summary section that provides an overview of the processes occurring at subauroral and high latitudes during this extreme storm.

4 Summary

This study comprehensively analyzes the dynamic interplay among the Storm-Enhanced Den-Sity (SED), the Tongue Of Ionization (TOI), and the Polar Ionospheric Hole (PIH) during the 10 May 2024 geomagnetic superstorm which produced the strongest geomagnetic disturbance in two decades, with *Dst* reaching ~ −500 nT. Global ionosphere experienced rapid, large-scale responses, including prompt penetration electric field (PPEF) effects on dayside and nightside. By utilizing global GNSS TEC and TIMED/GUVI [O]/[N_2] observations, we investigate how storm-time plasma structures at high altitudes evolved in response to thermospheric composition changes and polar cap convection. This event provides novel insights into the modulation and segmentation of TOI by coexisting PIH structures which signifies the presence of [O]/[N_2] depletion. Based on these observations, we outline the following scenario of processes at subauroral and high latitudes during the 10 May 2024 superstorm.

(1) With the arrival of ICME shock and subsequent B_z southward turning, PPEF generated a highly intense

fountain effect. This effect drove EIA crests moving poleward, causing a midlatitude density enhancement. At midlatitude, the poleward SAPS electric field provided significantly intensified sunward flow, while PPEF generated poleward flow, thus the two ion drift components led to the buildup of high electron density, forming the SED base and plume.

(2) At noon, the SED plume was entrained into the anti-sunward flow channel. This resulted in the TOI crossing the throat region and entering the polar cap.

(3) The PIH was formed, unusually on dayside at the beginning, as the neutral air with depleted [O]/[N_2] ratio began circulating in the morning sector toward noon. This presumed neutral circulation was primarily driven by the increased ion drag associated with significant auroral electric fields.

(4) Fresh TOI plasma is moving into the polar cap and rotating eastward, with some portion continuing moving in the antisunward direction. Following the TOI eastward convection, the PIH also rotates eastward.

(5) The PIH and TOI continued to be depleted, with TOI being segmented, as the entire polar cap was soaked by the neutral gas with substantially suppressed [O]/[N_2] ratio. The TOI and PIH remained eastward convicting for several hours, including a 2 h interval of larger positive IMF B_y.

Overall, this event underscores how neutral composition variability, especially with [O]/[N_2] de-pletion, can disrupt polar plasma transport and reshape TOI morphology and patches formation.

Acknowledgments This paper is dedicated to the late Prof. Zuo Xiao (1936–2025) of Peking University. It was there that SRZ began his journey in space science at the Department of Geophysics as an under-graduate and first encountered Prof. Xiao in the 1980 s. Prof. Xiao introduced him to Fortran programming, which played an instrumental role in his thesis work under Prof. Mingyun Zi and in his subsequent academic research. SRZ remains profoundly grateful for Prof. Xiao's enduring inspiration, generous guidance, and unwavering support throughout his career, as a dedicated mentor, an outstanding collaborator, a distinguished colleague who has left a lasting legacy in the field, and a kind and gracious elder.

GNSS TEC data processing and Madrigal database system (*http://cedar.openmadrigal.org) are provided to the community by MIT Haystack Observatory under the NSF grant AGS-2504079 support.

Data for TEC processing is provided from the following organizations: UNAVCO, Scripps Orbit and Permanent Array Center, Institut Geographique National, France, International GNSS Service, The Crustal Dynamics Data Information System (CDDIS), National Geodetic Survey, Instituto Brasileiro de Geografia e Estat'ıstica, RAMSAC CORS of Instituto Geográfico Nacional de la República Argentina, Arecibo Observatory, Low-Latitude Ionospheric Sensor Network (LISN), Topcon Positioning Systems, Inc., Canadian High Arctic Ionospheric Network, Institute of Geology and Geophysics, Chinese Academy of Sciences, China Meteorology Administration, Centro di Ricerche Sismologiche, Système d'Observation du Niveau des Eaux Littorales (SONEL), RENAG: REseau NAtional GPS permanent, GeoNet - the official source of geological hazard information for New Zealand, GNSS Reference Networks, Finnish Meteorological Institute, and SWEPOS - Sweden, Chinese Meridian Project, and International Meridian Circle Program (IMCP).

Ethical Approval This article does not contain any studies with human participants or animals performed by any of the authors.

Conflict of Interests The authors declare that there is no conflict of interests.

References

[1] FOSTER J C, COSTER A J, ERICKSON P J, *et al*. Multiradar observations of the polar tongue of ionization[J]. *Journal of Geophysical Research*: *Space Physics*, 2005, **110**(A9): A09S31

[2] HOSOKAWA K, TSUGAWA T, SHIOKAWA, K. et al. Dynamic temporal evolution of polar cap tongue of ionization during magnetic storm[J]. *Journal of Geophysical Research*: *Space Physics*, 2010, **115**: A12333

[3] THOMAS E G, BAKER J B H, RUOHONIEMI J M, *et al*. Direct observations of the role of convection electric field in the formation of a polar tongue of ionization from storm enhanced density[J]. *Journal of Geophysical Research*: *Space Physics*, 2013, **118**(3): 1180-1189

[4] LIU J, WANG W B, BURNS A, *et al*. Relative importance of horizontal and vertical transports to the formation of ionospheric storm-enhanced density and polar tongue of ionization[J]. *Journal of Geophysical Research*: *Space Physics*, 2016, **121**(8): 8121-8133

[5] ZOU S, RIDLEY A J, MOLDWIN M B, *et al*. Multi-instrument observations of SED during 24-25 October 2011 storm: implications for SED formation processes[J]. *Journal of Geophysical*

Research: *Space Physics*, 2013, **118**(12): 7798-7809

[6] ZOU S, MOLDWIN M B, RIDLEY A J, *et al*. On the generation/decay of the storm-enhanced density plumes: role of the convection flow and field-aligned ion flow[J]. *Journal of Geophysical Research*: *Space Physics*, 2014, **119**(10): 8543-8559

[7] Yuan, Z G, DENG X H, ZHANG S R, *et al*. F region behavior in the SED plume during a geomagnetic superstorm: A case study[J]. *Journal of Geophysical Research*: *Space Physics*, 2009, **114**: A08303

[8] ZHANG S R, ERICKSON P J, COSTER A J, *et al*. Subauroral and polar traveling ionospheric disturbances during the 7–9 September 2017 storms. *Space Weather*, 2019, **17**(1): 1748-1764

[9] FOSTER J C, BURKE W J. SAPS: a new categorization for subauroral electric fields[J]. *Eos, Transactions American Geophysical Union*, 2002, **83**(36): 393-394

[10] FOSTER J C, VO H B. Average characteristics and activity dependence of the subauroral polarization stream[J]. *Journal of Geophysical Research*: *Space Physics*, 2002, **107**(A12): 1475

[11] AA E, ERICKSON P J, ZHANG S R, *et al*. A statistical study of the subauroral polarization stream over north American sector using the millstone hill incoherent scatter radar 1979–2019 measurements[J]. *Journal of Geophysical Research*: *Space Physics*, 2020, **125**(10): e2020JA028584

[12] VALLADARES C E, BASU S, BUCHAU J, *et al*. Experimental evidence for the formation and entry of patches into the polar cap[J]. *Radio Science*, 1994, **29**(1): 167-194

[13] VAN-DER-MEEREN C, OKSAVIK K, LORENTZEN D, *et al*. GPS scintillation and irregularities at the front of an ionization tongue in the nightside polar ionosphere[J]. *Journal of Geophysical Research*: *Space Physics*, 2014, **119**(10): 8624-8636

[14] –ZHANG S R, ERICKSON P J, ZHANG Y L, *et al*. Observations of ion-neutral coupling associated with strong electrodynamic disturbances during the 2015 St. Patrick's day storm[J]. *Journal of Geophysical Research*: *Space Physics*, 2017, **122**(1): 1314-1337

[15] AA E, ZHANG S R, WANG W B, *et al*. Multiple longitude sector storm-enhanced density (SED) and long-lasting subauroral polarization stream (SAPS) during the 26-28 February 2023 geomagnetic storm[J]. *Journal of Geophysical Research*: *Space Physics*, 2023, **128**(9): e2023JA031815

[16] AA E, ZHANG S R, LEI J H, *et al*. Significant midlatitude plasma density peaks and dual-hemisphere SED during the 10-11 May 2024 super geomagnetic storm[J]. *Journal of Geophysical Research*: *Space Physics*, 2024, **129**(11): e2024JA033360

[17] DENG Y, RIDLEY A J. Role of vertical ion convection in the high-latitude ionospheric plasma distribution[J]. *Journal of Geophysical Research*: *Space Physics*, 2006, **111**(A9): A09314

[18] HUBA J D, SAZYKIN S, COSTER A. SAMI3-RCM simulation of the 17 March 2015 geomagnetic storm[J]. *Journal of Geophysical Research*: *Space Physics*, 2017, **122**(1): 1246-1257

[19] DANG T, LEI J H, WANG W B, *et al*. Formation of double tongues of ionization during the 17 March 2013 geomagnetic storm[J]. *Journal of Geophysical Research*: *Space Physics*, 2019, **124**(12): 10619-10630

[20] LU G, ZAKHARENKOVA I, CHERNIAK I, *et al*. Large-scale ionospheric disturbances during the 17 March 2015 storm: a model-data comparative study[J]. *Journal of Geophysical Research*: *Space Physics*, 2020, **125**(5): e2019JA027726

[21] ZHANG Q H, ZHANG B C, LOCKWOOD M, *et al*. Direct observations of the evolution of polar cap ionization patches[J]. *Science*, 2013, **339**(6127): 1597-1600

[22] ZHANG Q H, LOCKWOOD M, FOSTER J C, *et al*. Direct observations of the full Dungey convection cycle in the polar ionosphere for southward interplanetary magnetic field conditions[J]. *Journal of Geophysical Research*: *Space Physics*, 2015, **120**(6): 4519-4530

[23] WEBER E J, KLOBUCHAR J A, BUCHAU J, *et al*. Polar cap F layer patches: structure and dynamics[J]. *Journal of Geophysical Research*: *Space Physics*, 1986, **91**(A11): 12121-12129

[24] LOCKWOOD M, CARLSON JR H C. Production of polar cap electron density patches by transient magnetopause reconnection[J]. *Geophysical Research Letters*, 1992, **19**(17): 1731-1734

[25] ZHANG Q H, ZHANG B C, LIU R Y, *et al*. On the importance of interplanetary magnetic field $|B_y|$ on polar cap patch formation[J]. *Journal of Geophysical Research*: *Space Physics*, 2011, **116**(A5): A05308

[26] REN J, ZOU S, GILLIES R G, *et al*. Statistical characteristics of polar cap patches observed by RISR-C[J]. *Journal of Geophysical Research*: *Space Physics*, 2018, **123**(8): 6981-6995

[27] NISHIMURA Y, KELLY T, JAYACHANDRAN P T, *et al*. Nightside high-latitude phase and amplitude scintillation during a substorm using 1-second scintillation Indices[J]. *Journal of Geophysical Research*: *Space Physics*, 2023, **128**(8): e2023JA031402

[28] WANG Y, JAYACHANDRAN P T, ZHANG Q H, *et al*. Morphological comparison of standard scintillation indices at the Canadian arctic during a strong geomagnetic storm: a case study[J]. *Journal of Geophysical Research*: *Space Physics*, 2025, **130**(11): e2025JA034211

[29] BURNS A G, KILLEEN T L, WANG W, *et al*. A "tongue" of neutral composition[J]. *Journal of Atmospheric and Solar-Terrestrial Physics*, 2004, **66**(15-16): 1457-1468

[30] CAI X G, BURNS A G, WANG W B, *et al*. Investigation of a neutral " tongue" observed by GOLD during the geomagnetic storm on May 11, 2019[J]. *Journal of Geophysical Research*: *Space Physics*, 2021, **126**(6): e2020JA028817

[31] PRÖLSS G W. Ionospheric F-region Storms[M]//VOLLAND H. Handbook of Atmospheric Electrodynamics (1995). Florida: CRC Press, 2017

[32] BRINTON H C, GREBOWSKY J M, BRACE L H. The high-latitude winter *F* region at 300 km: thermal plasma observations from AE-C[J]. *Journal of Geophysical Research*: *Space Physics*, 1978, **83**(A10): 4767-4776

[33] JENNER L A, WOOD A G, DORRIAN G D, *et al*. Plasma density gradients at the edge of polar ionospheric holes: the absence of phase scintillation[J]. *Annales Geophysicae*, 2020, **38**(2): 575-590

[34] ZHANG S R, AA E. Ionospheric electron density large gradients at midlatitudes[M]//NISHIMURA Y, VERKHOGLYADOVA O, DENG Y, *et al*. Cross-Scale Coupling and Energy Transfer in the Magnetosphere-Ionosphere-Thermosphere System, Amsterdam: Elsevier, 2021.

[35] SPOGLI L, ALFONSI L, DE FRANCESCHI G, *et al*. Climatology of GPS ionospheric scintillations over high and mid-lati-

tude European regions[J]. *Annales Geophysicae*, 2009, **27**: 3429-3437

[36] THEMENS D R, ELVIDGE S, MCCAFFREY A, *et al*. The high latitude ionospheric response to the major May 2024 geomagnetic storm: a synoptic view[J]. *Geophysical Research Letters*, 2024, **51**(19): e2024GL111677

[37] RIDEOUT W, COSTER A. Automated GPS processing for global total electron content data[J]. *GPS Solutions*, 2006, **10**: 219-228

[38] VIERINEN J, COSTER A J, RIDEOUT W C, *et al*. Statistical framework for estimating GNSS bias[J]. *Atmospheric Measurement Techniques*, 2016, **9**(3): 1303-1312

[39] ZHANG S R, LIU J, COSTER A J, *et al*. Global GNSS observation of mesoscale ionospheric irregularities (2006-2024)[J]. *Journal of Geophysical Research*: *Space Physics*, 2026, **131**(3): e2025JA034951

[40] PRIKRYL P, GHODDOUSI-FARD R, SPOGLI L, *et al*. GPS phase scintillation at high latitudes during geomagnetic storms of 7-17 March 2012-Part 2: interhemispheric comparison[J]. *Annales Geophysicae*, 2015, **33**(6): 657-670

[41] SAITO A, FUKAO S, MIYAZAKI S. High resolution mapping of TEC perturbations with the GSI GPS network over Japan[J]. *Geophysical Research Letters*, 1998, **25**(16): 3079-3082

[42] TSUGAWA T, SAITO A, OTSUKA Y. A statistical study of large-scale traveling ionospheric disturbances using the GPS network in Japan[J]. *Journal of Geophysical Research*: *Space Physics*, 2004, **109**(A6): A06302

[43] DING F, WAN W, LIU L, *et al*. A statistical study of large-scale traveling ionospheric disturbances observed by GPS TEC during major magnetic storms over the years 2003-2005[J]. *Journal of Geophysical Research*: *Space Physics*, 2008, **113**(A3): A00A01

[44] ZAKHARENKOVA I, ASTAFYEVA E, CHERNIAK I. GPS and GLONASS observations of large-scale traveling ionospheric disturbances during the 2015 St. Patrick's day storm[J]. *Journal of Geophysical Research*: *Space Physics*, 2016, **121**(12): 12138-12156

[45] ZHANG S R, ERICKSON P J, GONCHARENKO L P, *et al*. Ionospheric bow waves and perturbations induced by the 21 August 2017 solar eclipse[J]. *Geophysical Research Letters*, 2017, **44**(24): 12067-12073

[46] SAVITZKY A, GOLAY M J E. Smoothing and differentiation of data by simplified least squares procedures[J]. *Analytical Chemistry*, 1964, **36**(8): 1627-1639

[47] COSTER A J, GONCHARENKO L, ZHANG S R, *et al*. GNSS observations of ionospheric variations during the 21 August 2017 solar eclipse[J]. *Geophysical Research Letters*, 2017, **44**(24): 12041-12048

[48] ZHANG S R, COSTER A J, ERICKSON P J, *et al*. Traveling ionospheric disturbances and ionospheric perturbations associated with solar flares in September 2017[J]. *Journal of Geophysical Research*: *Space Physics*, 2019, **124**(7): 5894-5917

[49] ZHANG S R, NISHIMURA Y, ERICKSON P J, *et al*. Traveling ionospheric disturbances in the vicinity of storm-enhanced density at midlatitudes[J]. *Journal of Geophysical Research*: *Space Physics*, 2022, **127**(8): e2022JA030429

[50] ZHANG S R, VIERINEN J, AA E, *et al*. 2022 Tonga volcanic eruption induced global propagation of ionospheric disturbances via lamb waves[J]. *Frontiers in Astronomy and Space Sciences*, 2022, **9**: 871275

[51] CHRISTENSEN A B, PAXTON L J, AVERY S, *et al*. Initial observations with the global ultraviolet imager (GUVI) in the NASA TIMED satellite mission[J]. *Journal of Geophysical Research*: *Space Physics*, 2003, **108**(A12): 1451

[52] STRICKLAND D J, MEIER R R, WALTERSCHEID R L, *et al*. Quiet-time seasonal behavior of the thermosphere seen in the far ultraviolet dayglow[J]. *Journal of Geophysical Research*: *Space Physics*, 2004, **109**(A1): A01302

[53] ZHANG Y, PAXTON L J, MORRISON D, *et al*. [O]/[N_2] changes during 1–4 October 2002 storms: IMAGE SI-13 and TIMED/GUVI observations[J]. *Journal of Geophysical Research*: *Space Physics*, 2004, **109**(A10): A10308

[54] ZHANG S R, NISHIMURA Y, VIERINEN J, *et al*. Simultaneous global ionospheric disturbances associated with penetration electric fields during intense and minor solar and geomagnetic disturbances[J]. *Geophysical Research Letters*, 2023, **50**(19): e2023GL104250

[55] HUANG F Q, LEI J H, YUE X N, *et al*. Interplay of gravity waves and disturbance electric fields to the abnormal ionospheric variations during the 11 May 2024 superstorm[J]. *AGU Advances*, 2025, **6**(1): e2024AV001379

[56] CHEN Y H, AA E, YUAN T J, *et al*. The extreme depletion of ionospheric electron density and its hemispheric asymmetry during the May 2024 storm[J]. *National Science Review*, 2025, **12**(10): nwaf307

[57] HUANG F Q, LEI J H, –ZHANG S R, *et al*. Peculiar nighttime ionospheric enhancements over the Asian sector during the May 2024 superstorm[J]. *Journal of Geophysical Research*: *Space Physics*, 2024, **129**(11): e2024JA033350

[58] SUN W j, LI G Z, ZHAO B Q, *et al*. Midlatitude plasma blob-like structures along with super equatorial plasma bubbles during the May 2024 great geomagnetic storm[J]. *Geophysical Research Letters*, 2024, **51**(21): e2024GL111638

[59] ZHANG S R, COSTER A J, ERICKSON P J, *et al*. Mesoscale ionospheric irregularity oval at high latitudes observed by global GNSS networks (2010-2024)[J]. *Journal of Astronomy and Space Sciences*, 2025, **42**(4): 119-134

[60] FORSYTHE V V, KUNDURI B, ZOU S. Multi-instrument investigation of the polar holes[J]. *Journal of Geophysical Research*: *Space Physics*, 2021, **126**(12): e2021JA029795

Author Biography



ZHANG Shun-Rong Dr. Shun-Rong Zhang, the first author and corresponding author, is a Principal Research Scientist at MIT Haystack Observatory. He has been actively involved in a diverse range of ionosphere and upper atmosphere research, encompassing geospace storm effects, variability, climatology, long-term changes, and the associated coupling processes in ionosphere-thermosphere-magnetosphere and atmospheric systems.
E-mail: shunrong@mit.edu